Carbon disulfide removal from gasoline fraction using zinc-carbon composite synthesized using microwave-assisted homogenous precipitation.

Ayat A.-E. Sakr (ayatsakr@yahoo.com)
Egyptian Petroleum Research Institute https://orcid.org/0000-0003-1987-0869
Noran Amr
MSA University: October University for Modern Sciences and Arts
Mohamed Bakry
Egyptian Petroleum Research Institute
Waleed El-Azab
Egyptian Petroleum Research Institute
Mohamed Ebiad
Egyptian Petroleum Research Institute

Research Article

Keywords: clean fuel, carbon disulfide, Zinc-carbon composite, urea hydrolysis, biomass, adsorption kinetics

Posted Date: November 21st, 2022

DOI: https://doi.org/10.21203/rs.3.rs-2176691/v1

Title:

Carbon disulfide removal from gasoline fraction using zinc-carbon composite synthesized using microwave-assisted homogenous precipitation.

Ayat A.-E. Sakr [a,*], Nouran Amr [b], Mohamed Bakry [a], Waleed I. M. El-Azab [a], Mohamed A. Ebiad [a]

Abstract

Carbon disulfide (CS_2) is one of the sulfur components that are naturally present in petroleum fractions. Its presence causes corrosion issues in the fuel facilities and deactivates the catalysts in the petrochemical processes. It is a hazardous component that negatively impacts the environment and public health due to its toxicity. This study used zinc-carbon (ZC) composite as a CS_2 adsorbent from the gasoline fraction model component. The carbon is derived from date stone biomass. The ZC composite was prepared via a homogenous precipitation process by urea hydrolysis. The physicochemical properties of the prepared adsorbent are characterized using different techniques. The results confirm the loading of zinc oxide/ hydroxide carbonate and urea derived species on the carbon surface. The results were compared by the parent samples, raw carbon, and zinc hydroxide prepared by conventional and homogeneous precipitation.

The CS_2 adsorption process was performed using a batch system at atmospheric pressure. The effects of adsorbent dosage and adsorption temperatures have been examined. The results indicate that ZC has the highest CS_2 adsorption capacity (124.3 $mg.g^{-1}$ at 30˚C) compared to the parent adsorbents and the previously reported data. The kinetics and thermodynamic calculations results indicate the spontaneity feasibility of the CS_2 adsorption process.

Keywords:

clean fuel; carbon disulfide, Zinc-carbon composite; urea hydrolysis; biomass; adsorption kinetics;

1. Introduction

According to EIA International Energy Outlook (2021) and B.P. Energy Outlook (2022), liquid petroleum fuels are considered the largest source of energy (EIA 2021; BP 2022). Petroleum or crude oil is composed mainly of hydrocarbon and may contain heteroatoms such as sulfur, oxygen, nitrogen, and metals. The type of crude oil can be classified according to the sulfur content, whether sweet or sour. Sour crude oil if it contains total sulfur of more than 0.5 wt%. Sulfur components have a corrosive action on pipelines, pumping, and refining equipment. Also, it deactivates the catalysts during the refining processes (Kohl and Nielsen 1997; Hsu and Robinson 2017; Saleh 2020). Different forms of Sulfur species may be present in petroleum which vary according to their origin, such as hydrogen sulfide (H_2S), carbonyl sulfide (COS), carbon disulfide (CS_2), mercaptans, sulfides, and thiophenes (Stumpf et al. 1998; Han et al. 2018; Saleh 2020).

Carbon disulfide (CS_2) is a type of sulfur component that can be present naturally in petroleum fractions such as gasoline (Stumpf et al. 1998; Rhodes et al. 2000; Yi et al. 2014). It is a non-polar linear molecule. When being pure, it is a colorless liquid with a pleasant smell. However, if it is impure, it has a pale yellow color, an offensive odor, and is considered a toxic chemical (Bocos-Bintintan and Ratiu 2020). It has many industrial applications, such as manufacturing viscous rayon, cellophane films, rubber, carbon tetrachloride, xanthates, thiourea, and mercaptans. It is a powerful solvent for materials such as resins, fates, rubbers, ….etc. (WHO 2002; DeMartino et al. 2017). Also, it can be used as an additive to the drilling mud to increase the efficiency of the hydraulic fracturing extraction of unconventional oil and gas (WHO 2002; Rich et al. 2016). However, it seriously impacts the environment and public health (Rhodes et al. 2000; Rich et al. 2016; Saleh 2020). It can be released into the atmosphere due to biological activities and anthropogenic actions such as burning fuel (petroleum, gas, coal) containing CS_2 (Bocos-Bintintan and Ratiu 2020). It is considered an indirect greenhouse gas, converted to CO_2, consequently increasing its amount in the atmosphere (Montero-Campillo et al. 2018). To meet the UN's sustainable development goals, (SDG 7 and 13) (UN 2015) for providing a clean source of energy and accelerating climate change mitigation; CS_2 must be removed during fuel processing.

Sulfur components can be removed from the fuels by different processes such as catalytic (hydro-or oxidative), biological, absorption by physical sorbents, or adsorption desulfurization (Speight

2011; Hsu and Robinson 2017; Sadare et al. 2017; Saleh 2020). It must be noted that the removal of the hydrogen sulfide (which is the major sulfur compound in the fuel) does not guarantee the removal of CS_2 (Dan et al. 2012). This is because it is much less acidic than H_2S, so conventional H_2S removal methods, such as physical solvents, do not effectively remove the CS_2 (Kohl and Nielsen 1997).

Among the desulfurization methods, we focused on adsorption desulfurization due to its advantages. It is economically viable; it can be performed at mild temperature and pressure conditions, the sulfur component can be recovered and utilized, and the adsorbent can be regenerated and reused (Chen et al. 2017; Iruretagoyena and Montesano 2018). Several adsorbents such as modified zeolites, metal-organic framework (MOF), activated carbon, metal oxides, e.g., Cu, Fe, Zn),.. etc., have been reported. (Ma et al. 2005; Guo et al. 2006; Chen et al. 2017; Iruretagoyena and Montesano 2018; Georgiadis et al. 2020; Wang et al. 2021).

Activated carbon is one of the most widely used adsorbents for pollutant removal, including gaseous and liquid contaminants. Coal, peat, wood, and various waste biomass are examples of carbonaceous substances employed as carbon precursors (Haggag et al. 2021). Date stones biomass contributes significantly to agricultural waste despite having little commercial value. According to the FAO, Egypt is also the world's top producer of dates (El-Sharabasy and Rizk 2019). Date stones usage as a carbon source is economically advantageous (Youssef et al. 2016; Ebiad et al. 2020).

ZnO has been reported previously as a desulfurization adsorbent at medium to high temperatures (Frilund et al. 2020; Georgiadis et al. 2020). Also, it was reported that CS_2 could react with primary and secondary amines (Kohl and Nielsen 1997). Zinc oxide can be synthesized by a homogeneous precipitation process using urea hydrolysis (Table S1) (Bitenc et al. 2008; Padmanabhan et al. 2009; Alhawi et al. 2015; Mantovani et al. 2017). Our previous studies indicated that controlling the urea hydrolysis conditions results in the insertion of nitrogen-containing anions (NH_2CO^-, isocyanate, or cyanate) within the structure of the adsorbent (Sakr et al. 2013, 2018, 2021).

In this work, we aimed to remove CS_2 from the gasoline fraction using Zinc hydroxide loaded on the surface of carbon material produced from biomass as an adsorbent. The synthesis and loading were performed in situ using homogeneous precipitation of zinc hydroxide by controlled urea hydrolysis with the assistance of microwave irradiation (as a green source of energy) (Baghbanzadeh et al. 2011)). These anions may affect CS_2 adsorption. The CS_2 removal was studied using a batch

adsorption system at low temperature and atmospheric pressure. To the best of our knowledge, there is no reported data considering the loading of Zn-based material on carbon surfaces using controlled urea hydrolysis. Also, there is no reported data about using this composite as an adsorbent of CS_2 from gasoline fraction (Table S2 and Table 2).

2. Material and methods

The chemicals used are; zinc nitrate, hexahydrate ($Zn(NO_3)_2.6H_2O$) (assay ≥ 99%), and urea (assay = 99%) purchased from Sigma-Aldrich. Ammonium hydroxide from Caledon Laboratories and heptane from CARLO ERBA. All chemicals are used without any further purification. The water was distilled and then deionized using LABCONCO, Water Pro (USA) deionizer.

2.1. Material Synthesis

Zinc materials were prepared either by conventional/ or homogenous precipitation pathways. The pH meter model pH-213 was used to measure the changes in pH in all of the synthesis reactions (Hanna, USA).

2.1.1. Synthesis of Zinc hydroxide by conventional precipitation method

To a solution containing zinc nitrate (0.05 M), ammonia solution (0.5 M) was added dropwise until the white precipitate was formed. The final pH reached 7.15. The precipitate (ppt) was then collected, centrifuged using MPW-352, Poland, and washed with deionized water several times. Then it dried in an oven at 80˚C.

2.1.2. Synthesis of Zinc hydroxide by homogenous precipitation method

This synthesis protocol is similar to our previous work (Sakr et al. 2018). In a typical synthesis, a solution containing zinc nitrate (0.05 M) and urea (0.5 M) was subjected to microwave irradiation (180 watts) in a domestic microwave oven for 90 min. The temperature reached 95 ˚C after 10 min and was constant along the reaction time. The synthesis reaction was done in an open glass vessel under atmospheric pressure. After the time for synthesis, the reaction was terminated immediately by cooling it down. As in step 1, the white formed ppt was centrifuged, washed, and dried.

2.1.3. Synthesis of Carbonized date stones

The carbon was prepared from Date stones, and the detailed synthesis method was described (Ebiad et al. 2020). The typical synthesis cleaned date stones (washed with distilled water) dried

at 105 °C and sieved from 1-2 mm. Then it is placed in a quartz tube inside a horizontal tube furnace (Nabertherm, Labothem Model R50/250/12; Germany) and heated up to 600 ˚C under nitrogen flow (100 ml/min) for 3 hrs. The obtained carbon was then ground and sieved.

2.1.4. Synthesis of Zinc-Carbon composite.

In a glass container, 2 g of the carbonized date stones were added to the solution containing zinc nitrate (0.05 M) and urea (0.5 M), then subjected to microwave irradiation. The same procedure was applied as in Step 2 to compare the results. A grey ppt is formed, collected and centrifuged, washed several times with deionized water, and dried at 80 °C. For simplicity, samples were coded as indicated in Table (1):

Table (1): The sample codes for the prepared adsorbents.

Sample Code	**Material**	**Synthesis method**	**Precipitating agent**	**Heating source**	**Synthesis Temperature**	**Final pH**
Z	zinc hydroxide	conventional precipitation	ammonium hydroxide	----	room temperature	7.15
ZU	zinc hydroxide	homogenous precipitation	urea	M.W.	95 °C	6.22
ZC	zinc-Carbon composite	homogenous precipitation	urea	M.W.	95 °C	6.01
C	carbonized date stones	calcination of date stones	---	horizontal tube furnace	600 °C	---

2.2. Characterization

The crystalline structures of the synthesized solids were analyzed by X-ray diffraction (XRD) (X Pert PRO, PANalytical, Netherlands) using Ni-filtered Cu Kα radiation operated at 40 kV. The spectra were recorded in an angular region of 2Θ = 4°–80° with a step size at 2Θ = 0.02° and a scanning step time of 0.6 sec.

The prepared adsorbents' Fourier transform infrared (FT-IR) spectra were analyzed using a Nicolet IS 50FTIR Spectrometer (Thermo-Fisher, USA). Each adsorbent was diluted with potassium bromide (KBr) and compressed in the form of a thin disc, and subjected to IR irradiation. The spectral wavelength region was from 4000 to 400 cm^{-1}.

The surface textural properties of the prepared adsorbents were characterized using nitrogen adsorption/desorption isotherm data obtained at 77˚K (NOVA, Quantachrome Instruments).

The surface morphology of the prepared adsorbents was examined using Field Emission Scanning Electron Microscope (Carl ZEISS, sigma VP 300). The instrument also allows Energy-dispersive Spectroscopy (EDS) using the Zeiss SmartEDX detector.

2.3 Adsorption activity:

The CS_2 adsorption ability of the prepared adsorbents was tested using a batch reactor (60 mL closed glass tube). A known amount of adsorbent was placed, mixed with a known volume of model component (heptane), representing the gasoline faction containing CS_2 with an initial concentration of 500 ppm. This mixture was stirred for 90 minutes (using a Thermo-scientific Stirrer, USA) at the required temperature. The CS_2 concentration was analyzed before and after the adsorption process using gas chromatography–chemiluminescence detector (GC-SCD), Agilent Technology, USA. The analysis method is performed according to the ASTM D5623 (D5623 2004) standard method, which is specified for analyzing sulfur compounds in low boiling point petroleum fractions.

The effect of temperature (30, 50, and 60˚C) on the adsorption process for all adsorbents under investigation is tested. Its dosage effect is tested for the most active adsorbent (20, 40, 60, 80, and 100 mg). The effect of time is also examined (60, 90, 120, 180, 210, and 240 min) at a working temperature of 30 °C.

The adsorption capacity was calculated as follows (Swat et al. 2017; Ebiad et al. 2020):

$$q = (C_0 - C)\frac{V}{w}$$

C_0 (mg/L) and C (mg/L) are the initial and at equilibrium solution concentrations of CS_2, respectively; V (L) is the volume of the solution, and **w (g)** represents the mass of adsorbents. The removal % can be calculated as follow:

$$\eta=(\frac{C_0-C}{C_0})100$$

3. **Results and Discussion**

3.1 pH change monitoring

The changes in the pH during the synthesis reaction of the Z.U. and ZC samples are discussed in detail in Section S1, Table S3, and Figures S1 and S2; in the supplementary file. Under MW irradiation, the urea hydrolysis reaction is affected by the presence of carbon particles in the synthesis

mixture (Figures S1 and S2). Also, the final pH is higher in the absence of the carbon sample. This may indicate that the released OH^- is consumed to neutralize the acid sites in the carbon surface as well as precipitate the zinc hydroxide.

It was reported that urea decomposes in aqueous media when subjected to heating (Shaw and Bordeaux 1955; Fernández et al. 2009) according to the following equation:

$$(NH_2)_2CO + 3H_2O \longrightarrow HCO_3^- + OH^- + 2NH_4^+$$

The release of the hydroxyl groups during the hydrolysis process is responsible for the precipitation of the Zn^{2+} ions in the form of zinc hydroxide or carbonate (Zhang and Li 2003). However, according to the synthesis conditions, several intermediate anionic groups could be formed, which in the end affects the structural features such as (carbamates, cyanates, isocyanates, and carbonates) (Saber and Tagaya 2005; Kloprogge et al. 2006; Mavis and Akinc 2006; Sakr et al. 2013, 2018, 2021; Faramawy et al. 2018)**.**

3.2 XRD analysis:

The XRD patterns of the prepared samples are represented in Figures 1 and S3. The XRD pattern for the (C) sample (Figure S3) shows the presence of two broad diffraction peaks at around 23.19 and 44.41 2Θ°, which correspond to the reflections of the (002) and (100) planes, respectively. The broadening and small intensity of the (002) plane may indicate the low degree of orientation of the aromatic layer in the three-dimensional aromatic carbon arrangement. While the broadening in the (001) plane may be related to the small aromatic layer slice in the carbon material (Qiu et al. 2019). This pattern indicates the presence of amorphous carbon with a low graphitization degree (Ebiad et al. 2020; Liu et al. 2021).

As indicated in Figure (1); the Z sample (prepared conventionally) exhibits the diffraction peaks at 15.40, 15.87, 17.02, 18.99, 25.99, 26.96, and 27.76 2Θ˚, revealing the presence of zinc hydroxide as compared to the zinc hydroxide (β-$Zn(OH)_2$) reference (JCPDS 20-1435). The diffraction peaks detected at 31.8, 34.6, 36.4, and 47.7 2Θ˚ correspond to ZnO as compared to the reference pattern (JCPDS 05-0664) of ZnO.

The XRD pattern for the ZU sample (papered by homogenous precipitation) shows presence diffraction peaks at 12.99, 24.03, 27.88, and 33.14 2Θ˚, in addition to 31.73, 34.37, 36.24, and 47.50 2Θ. It was observed that the latter diffraction angles are different in intensities compared to the **Z**

191 sample. This indicates the presence of hydrozinicite phase (zinc hydroxide carbonate, (JCPDS 14-
192 0256)) and a minor amount of ZnO ((JCPDS 05-0664), respectively. The low-intensity peak at 10.63
193 2Θ˚ could result from an anion other than carbonate (Sakr et al. 2013).

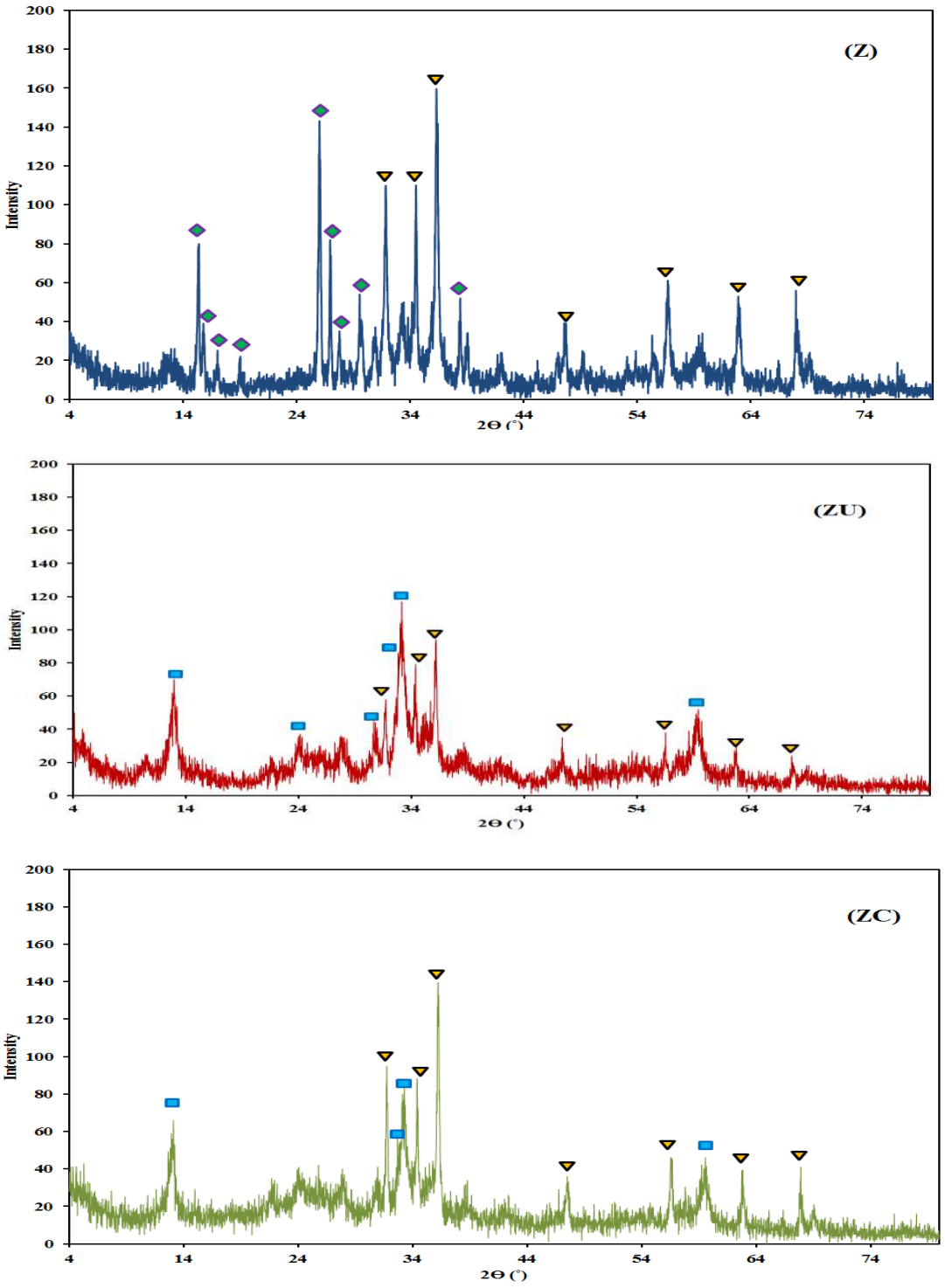

Fig. 1: XRD patterns for (Z), (ZU), and (ZC) materials. The shape (♦) represents the zinc hydroxide (β-$Zn(OH)_2$) phase, (▼) indicates the würtzite ZnO phase, and (■) for the hydrozinicite phase.

For the composite sample (ZC), the XRD pattern resamples that of the ZU sample and reveals the hydrozinicite phase (zinc hydroxide carbonate, (JCPDS 14-0256)) and ZnO ((JCPDS 05-0664), respectively. The main difference was the relatively high intensity of the peak at 36.23 2Θ˚, corresponding to the (101) phase. This may suggest that the presence of carbon samples in the precipitation media affects the ZnO phase formed on the carbon surface and results in phases having different aspect ratios. The disappearance of the characteristic peaks of the amorphous carbon in the C sample may indicate the homogenous surface coverage of the carbon material by the Zn oxide/hydroxide carbonate species.

3.3 FTIR spectra

The IR spectra of the Zinc-containing samples are presented in Figure (2).

1- For the Z sample:

The structural vibrational region shows an absorption band at 481 $cm^{-1,}$ corresponding to the Zn-O bond stretching vibration in ZnO nanorods (Bundit and Wongsaprom 2018). The presence of the split peaks 514 and 431 cm^{-1} indicates the presence of another morphology of particles (Verges et al. 1990).

A broad band in the region 3000- 4000 cm^{-1} corresponds to the hydrogen-bonded hydroxyl groups. The 1507 cm^{-1} and 1392 cm^{-1} (with the shoulder at 1363 cm^{-1}) correspond to the vibration of hydroxyl groups bonded to Zn atoms and water (Giannakoudakis et al. 2015). The presence of 1363 cm^{-1} could result from C=O vibration from adsorbed CO_2 on the surface. The band at 1041 cm^{-1} is assigned to Zn-OH bending vibration. The OH deformation band is detected at 830 cm^{-1} (Giannakoudakis et al. 2015).

This sample is prepared in an ammonia solution at room temperature. The reaction formation steps could be as follow (Zhang et al. 2007).

$$NH_4OH \longrightarrow NH_3^+ + OH^-$$

$$Zn^{2+} + 4NH_3^+ \longrightarrow Zn(NH_3)_4^{2+}$$

$$Zn(NH_3)_4^{2+} \longrightarrow ZnO + 4NH_3 + H_2O$$

$$Zn^{2+} + 4OH^- \longrightarrow Zn(OH)_4^{2-}$$

$$Zn(OH)_4^{2-} \longrightarrow ZnO + H_2O + OH^-$$

It was reported that below pH 7 and temperature less than 60˚C, the formation of ZnO particles is slowed down (Zhang et al. 2007). In this work, a small amount of ZnO is observed. The spectral data is consistent with the XRD pattern of the Z sample.

2- For ZU sample

The IR spectrum for the ZU sample is represented in Figure (2). The absorption band at 415 cm^{-1} could correspond to the starching vibrational mode of the octahedral Zn_o-O cluster (Gordeeva et al. 2020). The absorption band at 467 cm^{-1} corresponds to the Zn-OH translation vibration in the hydrozincite structure (Kloprogge et al. 2004)**.**

The bands at 1550, 1386, and 732 cm^{-1} could correspond to the vibration modes of carbonate groups. The presence of split at 1364 cm^{-1} could be due to the different modes of symmetric vibration of carbonate anion (bidentate) (Padmanabhan et al. 2009; Sakr et al. 2018). The broad band centered at 3385 cm^{-1} indicates the presence of hydrogen-bonded adsorbed water molecules with surface hydroxyl groups. The spectrum also exhibits a small absorption band at 2202 cm^{-1}, corresponding to the cyanate group's presence. The cyanate group is formed due to incomplete urea hydrolysis under the reaction conditions (Sakr et al. 2013).

The above results indicate the formation of the hydrozincite phase as well as of the zinc oxide phase. These results are in agreement with that observed by Padmanabhan et al. (2009), who stated that; an amorphous intermediated $Zn(OH)_2$ could be formed and transformed into the ZnO as a result of the synthesis conditions (Padmanabhan et al. 2009).

3- For ZC composite sample

The IR spectrum of the Sample (ZU) resembles that of Sample (ZC) (Figure 2). However, the structural vibration region shows a little shift in the bands 514 cm^{-1} and 418 cm^{-1} in Sample Z to be 499cm^{-1} and 408 cm^{-1} in sample ZC, which could indicate the presence of another particle morphology like prism formation (Verges et al. 1990).

The vibrational region characteristic to the formed anions confirming the presence of carbonate anions is detected with the characteristic band at 1386 cm^{-1} with a small shoulder at 1364 cm^{-1} (compared to that of the Z.U. sample). This may indicate that the monodentate carbonate anions present on the composite surface is predominating. The presence of urea-

derived anions is also detected in the form of a cyanate group with a peak centered at 2208 cm^{-1}.

The FTIR results are in agreement with those obtained from the XRD data. Under the synthesis conditions, the formed composite contains the Zinc oxide/ hydroxide carbonate with the presence of urea-derived anions as well.

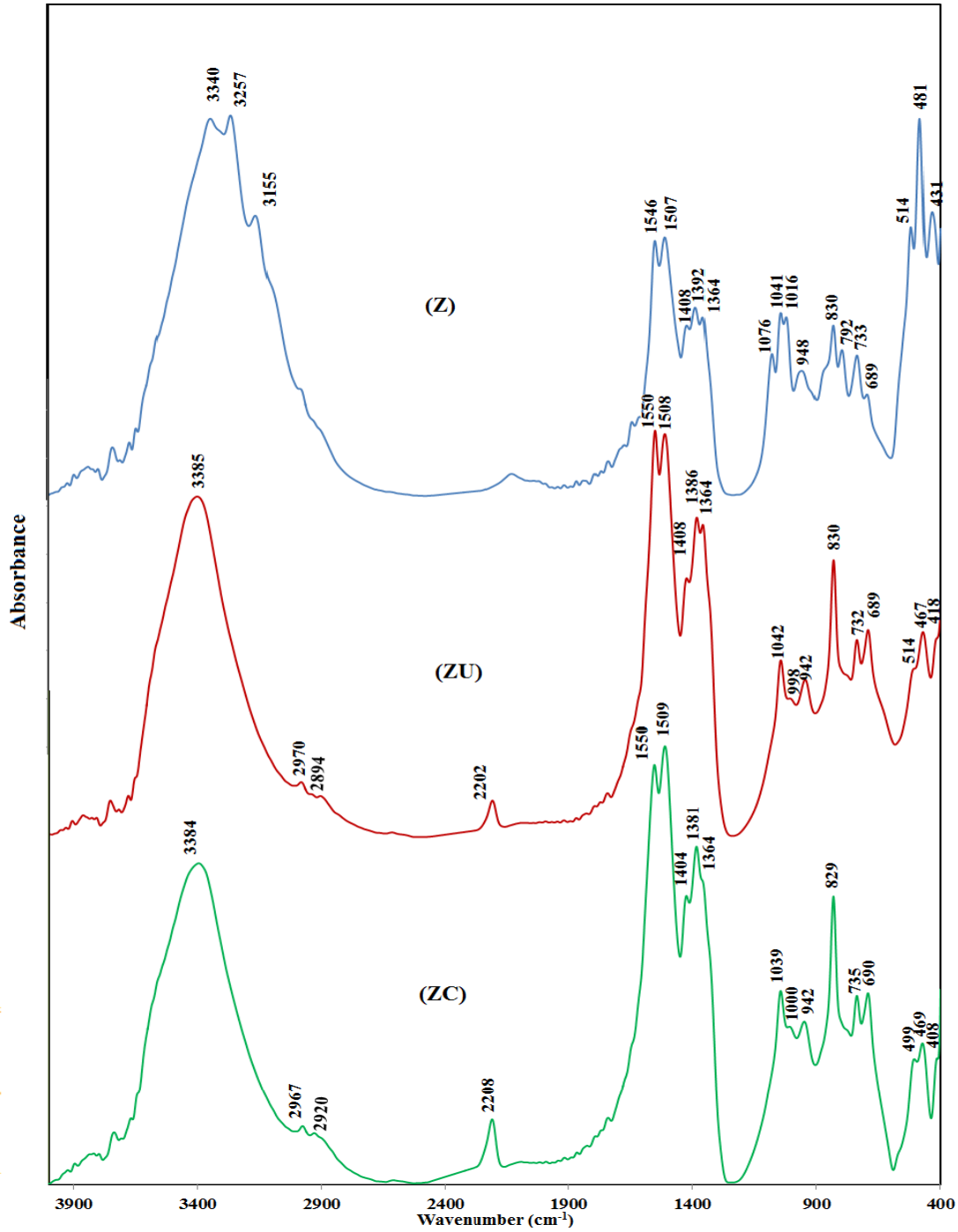

Fig. 2: FTIR spectra for Z, ZU, and ZC materials.

3.4 Field emission scanning electron microscope (FESEM) Images.

The morphology of the prepared solids is shown in the FESEM images represented in Figure (3). The C material shows irregular aggregates of stacked sheets (Figure 3a). The Z material shows the formation of semispherical and rode-like particles (Figure 3b). Whereas the ZU sample images (Figure 3c) indicate the presence of flakey-like particles (Padmanabhan et al. 2009) aggregated in large spherical particles. This is consistent with Molefe et al. (2015), who stated that temperature could act as a structural directing agent to gather the sphere-like particle to form a larger flak-like one (Molefe et al. 2015).

The particles of the ZC sample appeared in the form of a prism shape as well as flaky-like particles that coated the carbon particles (Figure 3d). These data are confirmed from the EDS analysis of the ZC sample Figure (S5), which reveals the formation of the Zn-carbon composite. The data from the FESEM images agree with those obtained from the XRD and FTIR results.

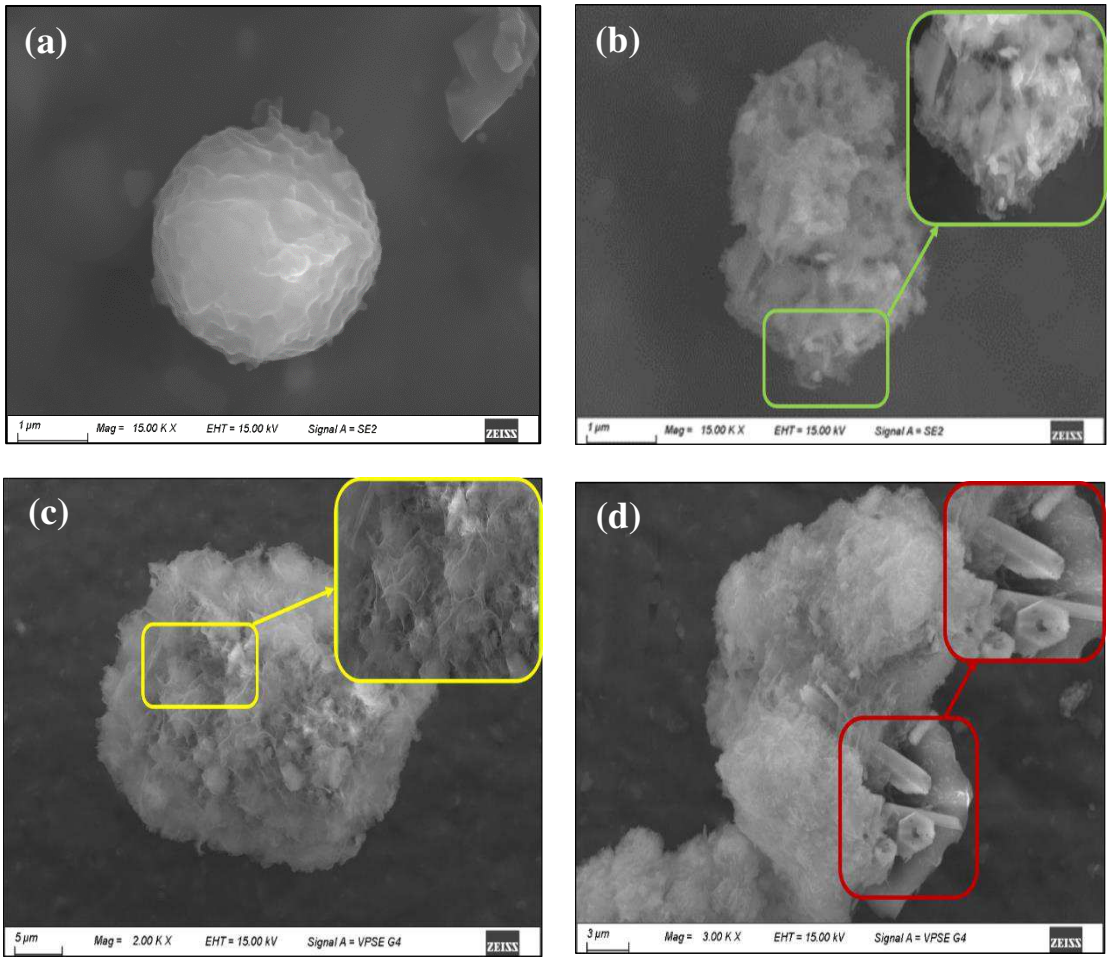

Fig. 3: FESEM images for a) C, b), Z, c) ZU, and d) ZC materials.

3.5 Surface textural properties:

The textural characteristics of the prepared materials were tested using the nitrogen adsorption-desorption isotherm at low-temperature Figures (4 and S6) and Table (S4). The specific surface area was calculated according to Brunauer-Emmett-Teller (BET) method. The pore size distribution and pore volume were calculated from the desorption curve in the isotherm using the Barrett-Joyner. Halenda (BJH) model.

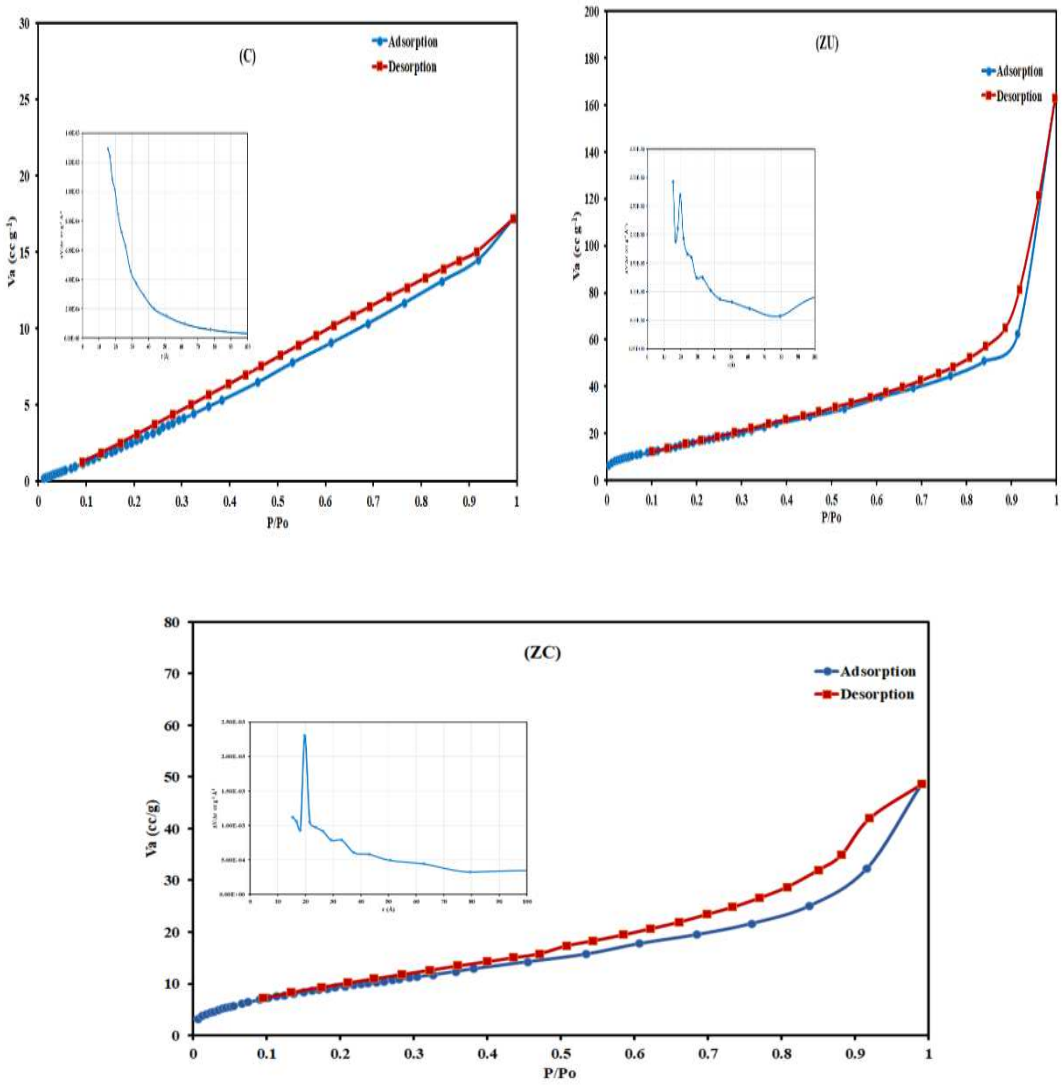

Fig. 4: The N_2 adsorption-desorption isotherm for C, ZU, and ZC materials. The insert figures indicate the BJH pore size distribution corresponding to each material.

The isotherm of the C sample reveals the presence of type III isotherm (according to the International Union of Pure and Applied Chemistry (IUPAC) classification), which indicates the presence of silt-like pores formed from the aggregation of plate-like particles (Ramimoghadam et al. 2013). The hysteresis indicates the presence of some mesoporosity that may be formed due to the

aggregation of the particles. The BET surface area of the C sample was 26.89 m^2 g^{-1}. After loading with zinc hydro(oxide) particles, the BET surface area is slightly increased to 35.64 m^2 $g^{-1,}$ which could be due to the C particle acting as a nucleus that helps the formation of a web or network from the Zn hydro(oxide) particles on its surface (Seredych et al. 2012; Giannakoudakis and Bandosz 2014). The surface area of the ZC is an intermediate between that of the C and ZU sample, indicating the Zn material's loading on the C surface (Mantovani et al. 2017) and confirming that obtained from the FE-SEM results. The isotherm of ZC samples is type IV with H3 hysteresis, which indicates mesoporosity due to the aggregation of the formed layered particles (Guo et al. 2016).

The BJH model was used to calculate the average pore size distribution (PZD) results, which show that the C sample has a PSD of <15.33 Å, while the ZU sample has two modes of the pore size distribution (<15.37 and 19.77 Å). The ZC sample possesses a narrow PSD of 19.75 Å. All the prepared solids show a PSD in the mesopore range which gives them an advantage in the adsorption of organic pollutants (Han et al. 2006).

3.6 Adsorption Activity

The adsorption capacity was calculated as follows (Swat et al. 2017; Ebiad et al. 2020):

$$q = (Co - C)\frac{V}{w} \quad (1)$$

Co (mg/L) and C (mg/L) are the initial and at equilibrium solution concentrations of CS_2, respectively; V (L) is the volume of the solution, and w (g) represents the mass of adsorbents. The removal % can be calculated as follow

$$\eta = (\frac{Co-C}{Co})100 \quad (2)$$

The adsorption process was carried out using a batch reactor at atmospheric pressure. The CS_2 adsorption capacities are shown in Figure (5) at 30 °C and constant weight of 20 mg. The data reveal that the adsorbents for capture CS_2 from the gasoline model component follow the order of C (91.6) < Z (118.2) < Zu (122) < ZC (124.3 mg(CS_2)/g(adsorbent)).

The maximum adsorption capacity was found to be by the ZC adsorbent with an adsorption capacity of 124.3 mg (CS_2)/g(adsorbent) with 49.7%. The obtained data is higher than reported in the literature using the adsorption technique at low temperatures (Table 2)

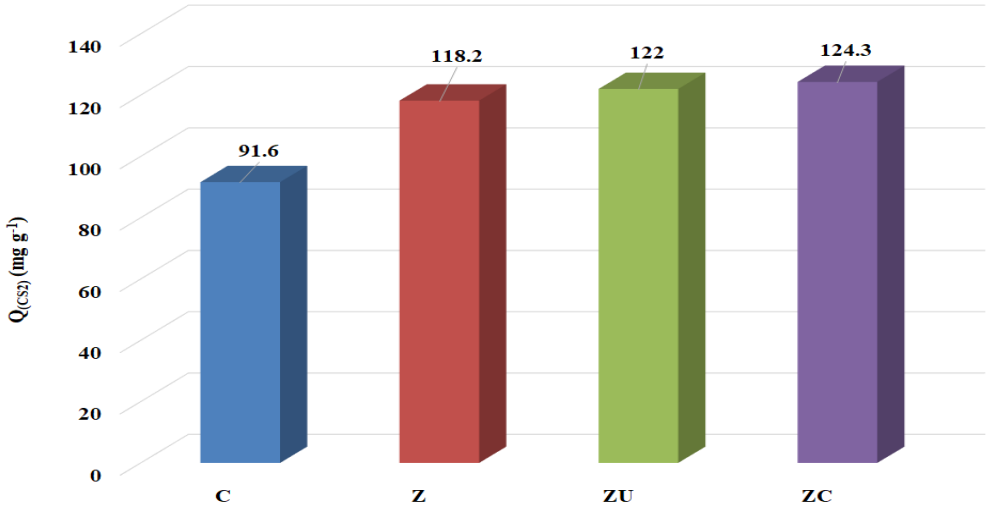

Figure (5): CS_2 adsorption capacity diagram at 30˚C for the tested adsorbents.

Table 2: Previously reported data on CS_2 adsorption by activated carbon.

Type of material	Reaction	Adsorption capacity	Temperature	Source	Reference
Zinc-carbon composite	Batch reactor	124.3 mg of CS_2/g	30˚C	hydrocarbon	This work
Cu/CoSPc/Ce Modified Activated Carbon ($AC_{Cu\text{-}CoSPc\text{-}Ce}$)	fixed-bed quartz reactor system	adsorption capacity of 17.39 mg of CS_2/(g of activated carbon)	20 °C	Gas	(Wang et al. 2014)
Activated carbons	Batch system	the adsorption capacity of CS_2 in damp gas is 60%–80% less than that in dry gas	50 °C	Gas	(Wang et al. 2011)
Active carbon fiber (ACF)	Batch system	The adsorption capacity of ACF is more extensive (72–104%) than that of GAC	150 °C	water	(Yang et al. 2006)
Ion-exchanged zeolites Y	fixed-bed adsorption column	the highest CS_2 breakthrough adsorption capacity up to 44.8 mg/g.	20 °C	Air	(Chen et al. 2017)
Polyacrylonitrile (PAN)-based activated carbon fiber (ACF)	a fixed-bed glass reactor	The best breakthrough adsorption capacity of CS_2 was 55.63 mgS/g when CO activated the ACF	Room temperature	N_2 gas	(Li et al. 2020)
Hydrophobisation of activated carbon fiber (ACF) using vinyltrimethoxysilane	glass vacuum system	The adsorption selectivity is improved under humid conditions	25 °C	N_2 gas in dynamic conditions	(Xie et al. 2011)
Activated carbon modified with KOH and ethylenediamine	glass vacuum system	The CS_2 adsorption is improved	30-60 °C /0–30,000 Pa.	--	(Guo et al. 2006)

This higher reactivity could be due to the surface texture of the prepared Zn-carbon composite, where the basic surface nitrogen species are formed during the urea hydrolysis and confirmed by the IR and XRD. This conclusion is supported by those reported previously (Kohl and Nielsen 1997; Guo et al. 2006; McGuirk et al. 2018; Orhan et al. 2019; Cao et al. 2020), where the

presence of a nitrogen-containing group enhances the CS_2 adsorption. In addition, the presence of the hydroxycarbonate group on the surface due to the urea hydrolysis reaction contributes to the CS_2 adsorption (Kowalik et al. 2020). Also, CS_2 can be physically adsorbed on the ZnO surface (Sahibed-Dine et al. 2000). In this work, the morphology of the ZnO oxide species with a prism shape on the surface of carbon particles in the ZC adsorbent may positively affect the CS_2 adsorption process. This is in agreement with Ghenaatian et al. (2013), who confirmed that the structural morphology of the ZnO particles plays an important role in the CS_2 capture and storage process(Ghenaatian et al. 2013).

Figure (6) depicts the effect of the adsorbent dose on the adsorption process at 30 °C. It was observed that the adsorption capacity decreased with increasing the mass of the adsorbent. This may be due to the aggregation and accumulation of the adsorbent particles, which could hinder the active site of the adsorbent, making it less accessible to the CS_2 molecules (Wang et al. 2010).

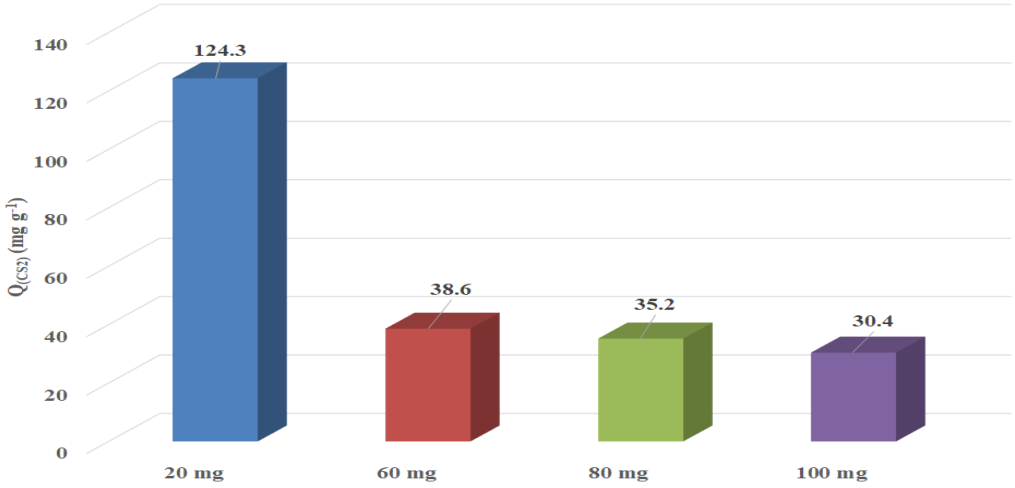

Fig. 6: Effect of ZC adsorbent dose on the CS_2 adsorption capacity.

3.7 Adsorption Kinetics

We studied the kinetic behavior of CS_2 adsorption onto ZC adsorbent at a working temperature of 30 °C and atmospheric pressure, considering the effect of time on the adsorption process (Figure 7a). The CS_2 adsorption increased quickly at first with time, then slowed down until equilibrium was reached. This increase may be due to the high concentration of CS_2 and free active sites on the adsorbent surface between 0 and 120 minutes. Following that time, the number of available

free active sites on the adsorbent surface became limited, resulting in a gradual decrease in the adsorption process.

Studying the adsorption process kinetics indicates its efficiency and applicability to process scaling up (Doğan et al. 2009). Two main kinetic model groups describe the adsorption reaction. The first, models that could predict adsorption reaction through the adsorption rate on the adsorbent surface, and the second could predict the adsorption mechanism (Ebelegi et al. 2020).

Pseudo-first order and pseudo-second order are the two widely used kinetic models that could be applied to the experimental adsorption data to assess adsorption reaction kinetics. The pseudo-first-order model of adsorption's differential form can be written as follows (Lagergren 1898):

$$\frac{dq_t}{dt} = k_1(q_e - q_t) \quad (3)$$

Where k_1 is the equilibrium constant (min^{-1}) and q_e and q_t ($mg.g^{-1}$) are the amounts of CS_2 adsorbed at equilibrium and at time t, respectively. Using Eq. (3)'s integration and the initial conditions $q_t = 0$ at $t = 0$

$$\log (q_{e1} - q_t) = \log q_{e1} - (\frac{k_1}{2.303})\, t \quad (4)$$

The pseudo-second-order reaction equation's differential version can be expressed as (Ho and Mckay 1999):

$$\frac{dq_t}{dt} = k_2(q_e - q_t)^2 \quad (5)$$

Where k_2 ($mg.g^{-1}.min^{-1}$) is the pseudo-second rate constant. The linearized form of this model is produced after integration, taking the boundary conditions into account as follows:

$$\frac{t}{q_t} = \frac{t}{q_{e2}} + \frac{1}{k_2 q_{e2}^2} \quad (6)$$

From the results listed in Table (3)and Figure 7 (b & c), the pseudo-second-order (PSO) kinetic model offers the best agreement between the estimated values of q_{e2} and the experimental q_e data, with a high correlation coefficient of 0.9895. These findings imply that the PSO kinetic model was followed by the CS_2 adsorption process on the ZC adsorbent. This alludes to the fact that chemisorption, which involves valence forces through sharing (covalent force) or exchange of electrons

between sorbent and sorbate, regulates the adsorption process (Haggag et al. 2021). These results may reflect the role of the active sites, including the nitrogen-containing anions and Zn-species loaded on the carbon surface during the CS_2 adsorption process.

Mechanism of adsorption

Three steps are typically used to illustrate the adsorption mechanism (Youssef et al. 2014); i) film diffusion is the transfer of adsorbate molecules from the main body of the solution to the adsorbent's surface, ii) ions are moved from the surface to the intraparticle active sites (particle diffusion), and iii) ions are adsorbed by the adsorbent's active sites. The third step does not fall within the rate-controlling phases because it is a relatively quick process. Therefore, either film diffusion or particle diffusion is primarily responsible for the rate-controlling stages. Weber and Morris are the first to descript the intraparticle diffusion model. They illustrated that uptake during adsorption was proportional to the square root of the contact time (Weber and Morris 1963)

$$q_t = K_{id}\, t^{0.5} + C_i \qquad (7)$$

K_{id} is the intraparticle diffusion rate constant [$mg.g^{-1}$ $(min^{0.5})^{-1}$]. While C is the intercept, the value of K_{id} is determined by the slope of the straight line (Figure 7d). The thickness of the boundary layer is evaluated by the value of C. The boundary layer effect increases with increasing intercept C. Table 3 provides the results of the variables K_{id}, C, and R^2.

Table (3): Kinetic parameters for the adsorption of CS_2 onto C.Z. sample at 30 °C

Model	Constant parameter	30 °C
	$q_{e,exp}$ ($mg.g^{-1}$)	85.096
Pseudo first order	q_{e1} ($mg.g^{-1}$)	8.758
	k_1 ($L.min^{-1}$)	0.0187
	R^2	0.9737
Pseudo second order	q_{e2} ($mg.g^{-1}$)	128.205
	k_2 ($g.\ mg^{-1}.\ min^{-1}$)	2.78E-5
	R^2	0.9895
Intraparticle diffusion	K_{ip}	8.044
	C	-20.39
	R^2	0.9909
Boyd plot	Intercept	-0.9394
	R^2	0.9896

The dual linear regions of this curve, according to this concept, can be attributed to the different adsorption extents at the beginning and final stages. The second region section rises gradually with the intraparticle diffusion, while the first steep one represents the exterior surface adsorption. The plot of q_t vs. $t^{1/2}$ should be linear and pass through the origin if intraparticle diffusion is the rate-limiting step. None of the intraparticle diffusion plots crossed through the origin, indicating that the intraparticle diffusion mechanism is not the only rate-controlling step and the film diffusion had an impact as well (boundary layer diffusion).

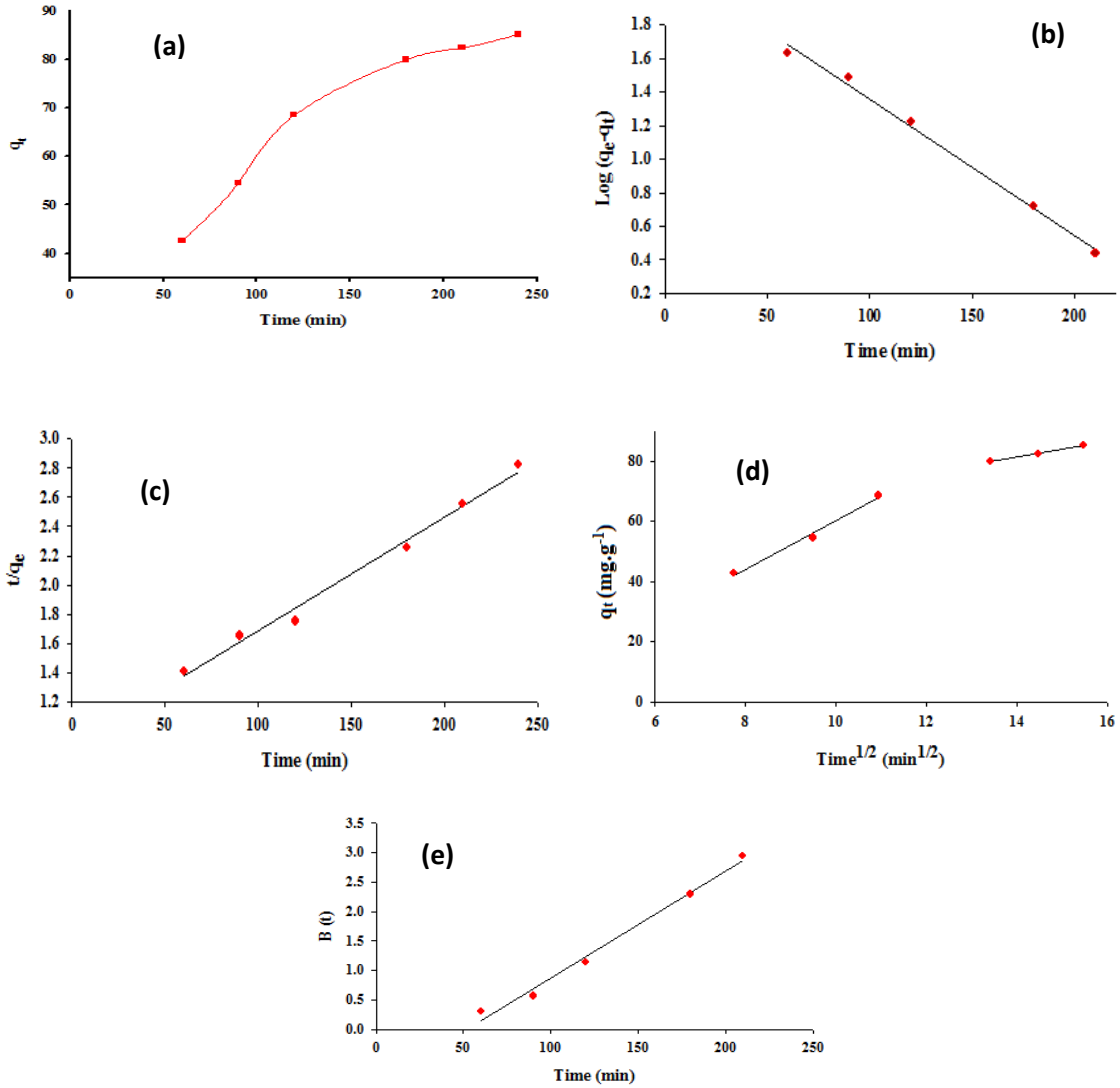

Fig. 7: **a)** Effect of time on CS_2 adsorption by ZC sample at 30°C, **b)** Pseudo-first-order kinetic model for adsorption, **c)** Pseudo-second-order kinetic model, **d)** Intraparticle diffusion plots, and **e)** Boyd plots for CS_2 adsorption.

The kinetic data were subsequently examined using the Boyd kinetic model to discriminate between film diffusion and particle diffusion to forecast the slow step involved. The Boyd kinetic equation (Boyd et al. 1947) is denoted as:

$$F(t) = 1 - \frac{6}{\pi^2}\sum_{n=1}^{\infty}\frac{e^{-n^2Bt}}{n^2} \qquad (7)$$

Where F is the fractional attainment of the equilibrium at a different time (t), and B(t) is a mathematical function of F.

$$F = \frac{q_t}{q_e} \qquad (8)$$

Where q_t and q_e are the amount adsorbed at the time (t) and equilibrium, respectively.

Reichenberg was successful in getting the following estimates (Reichenberg 1953):

For F values > 0.85 $\quad B(t) = -0.4977 - \ln(1 - F) \qquad (9)$

And for F values < 0.85 $\quad B(t) = \left(\sqrt{\pi} - \sqrt{\pi - \left(\frac{\pi^2 F(t)}{3}\right)}\right)^2 \qquad (10)$

Investigating the linearity of the experimental value and the data listed in Table (3) by plotting B(t) against time t as depicted in Figure (7e). Particle-diffusion mechanisms govern the adsorption process if the plots are linear and pass through the origin. According to the findings, film diffusion governs the adsorption of CS_2 on the ZC sample at 30 °C. because the plot line does not pass through the origin Figure(7e) (Chen et al. 2010).

3.8 Adsorption thermodynamics

Figure (7) shows the effect of temperature on the CS_2 adsorption capacity using ZC as an adsorbent with constant weight (20 mg) and atmospheric pressure. The data indicate that the capacity slightly decreased with increasing temperature in the physical adsorption process. The adsorption process is exothermic; consequently, it is favored at low temperatures (Wang et al. 2015). These results are assisted with the thermodynamic calculation. Taking the thermodynamic consideration is important to evaluate the feasibility and spontaneity of the adsorption process (Ebelegi et al. 2020).

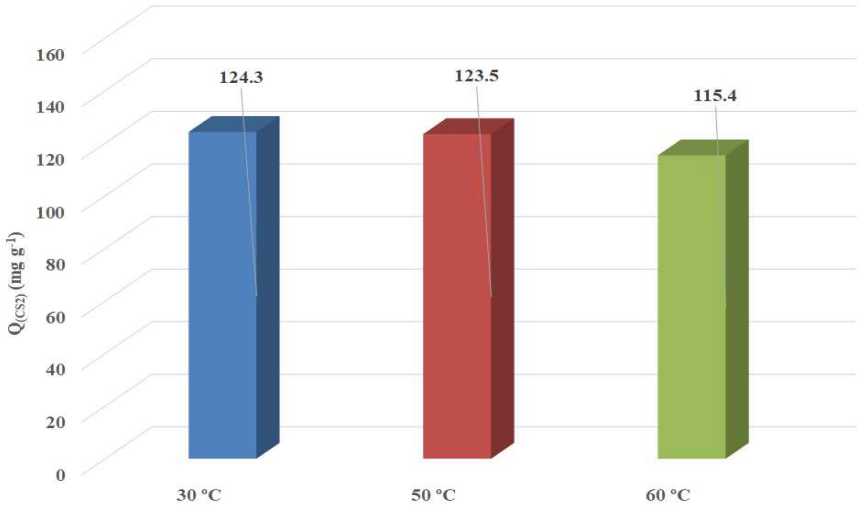

Fig. 7: Effect of temperature on the CS_2 adsorption capacity using ZC adsorbent.

Thermodynamic parameters such as Gibbs free energy (ΔG^o), entropy (ΔS^o), and enthalpy (ΔH^o) were calculated using the following equations:

$$K_d = \frac{C_s}{C_e} \quad (11)$$

$$\Delta G^o = \Delta H^o - T\Delta S^o \quad (12)$$

$$ln\ K_d = \frac{\Delta S}{R} - \frac{\Delta H}{RT} \quad (13)$$

Where C_e is the equilibrium concentration ($mg.L^{-1}$) of CS_2 in the solution, Kd is the adsorption distribution coefficient, and C_s is the quantity of CS_2 adsorbed on the adsorbent surface per liter of the solution at equilibrium. R, the gas constant, and T, the temperature. The slope and intercept of Van't Hoff plots of (ln K_d) vs. 1/T were used to derive ΔH^o and ΔS^o.

Table 4: Thermodynamic parameters for CS_2 adsorption on ZC sample at 30 °C, 50 °C, and 60 °C

Sample	ΔH° (kJ.mol^{-1})	ΔS° (kJ.mol^{-1} K^{-1})	ΔG° (kJ.mol^{-1})			K_d		
			303 K	323 K	333 K	303 K	323 K	333 K
ZC	1.77	0.0116	-1.76	-1.89	-2.14	2.012	2.024	2.166

The negative ΔG° values represent the spontaneous adsorption of CS_2 onto the ZC adsorbent, according to the thermodynamic characteristics shown in Table (4). The adsorption of CS_2 onto the ZC sample could be categorized as physisorption adsorption, with the change in free energy for this

process ranging between -2.14 and -1.76 kJ.mol^{-1}. It was reported that the ΔG° for chemisorption ranges between -80 and -400 kJ.mol^{-1} and that for physisorption ranges from -20 to 0 kJ.mol^{-1} (Ebiad et al. 2020).

The positive ΔH° values (1.77 kJ.mol^{-1}) indicate that the adsorption of CS_2 is endothermic. The ΔS° calculated positive values for ZC sample 0.0116 kJ.mole^{-1} K^{-1}. These show an increase in unpredictability at the interface between the solid and the solution. To break through the activation energy barrier and increase the intraparticle diffusion rate, mobility must be increased. Based on the adsorption kinetic and thermodynamic results, it can be concluded that the CS_2 adsorption on the Zn-carbon composite is a spontaneous and feasible process.

4. Conclusion

In this study, carbon from date stone biomass was used to form carbon material that can be used as a CS_2 adsorbent. Zinc hydroxide was in-situ synthesized and loaded on the carbon surface using a homogeneous precipitation process by urea hydrolysis. The synthesis reaction was assisted by microwave irradiation. Different techniques characterized the resulting zinc-carbon composite to elucidate its structure characteristics. It was found that flake-like zinc hydroxide particles were formed on the carbon surface, making a net-like morphology. Also, zinc oxide particles in the shape of a prism were recognized. This reflects the role of the presence of carbon particles in the synthesis reaction media.

The efficiency of the prepared zinc-carbon composite in removing CS_2 from light petroleum fraction was tested. For comparison, the conventional zinc hydroxide (precipitated by NH_4OH) and Zinc hydroxide (precipitated) by urea hydrolysis) as well as raw carbon was characterized, and their adsorption activities were tested. The adsorption process was done in a batch reactor at atmospheric pressure. The effect of temperature and adsorbents' dose on adsorption was examined. Kinetics studies stated that the pseudo-second-order kinetic model successfully fitted the experimental data and the rate-determining step in the adsorption process of the ZC sample at 30 °C.

Moreover, the adsorption mechanism governs by film diffusion. The determination of the thermodynamic parameters (ΔG^o, ΔH^o, and ΔS^o) showed that CS_2 spontaneously adsorbs onto the ZC adsorbent due to the negative values of ΔG^o. Additionally, a positive change in enthalpy shows that the adsorption process was endothermic. The enhanced unpredictability at the solid/solution interface increases the adsorption process, as seen by the positive entropy values for the ZC sample. The best

adsorption capacity (124.3 mg (CS_2)/g) was for zinc-carbon composite at 30 °C and atmospheric pressure. The results were higher than those reported in the previous studies. From the obtained results, the CS_2 adsorption on the Zn-Carbon composite process is spontaneous and feasible.

Supporting Information

Supporting Information is available.

Acknowledgments

The authors would like to greatly thank the teams of EPRI Central Labs for their support during this research.

Funding

- This research work did not receive any specific grant from the public, commercial, or not-for-profit funding agencies.
- Open access funding provided by The Science, Technology & Innovation Funding Authority (STDF) in cooperation with The Egyptian Knowledge Bank (EKB).

***Author Contributions*:**

***Ayat A.-E. Sakr**:* Conceptualization; Data curation; Formal analysis; Investigation; Methodology; Supervision; Visualization; Roles/Writing - original draft; Writing - review & editing. ***Nouran Amr**:* Formal analysis; Investigation; Methodology. ***Mohamed Bakry**:* Conceptualization; Data curation; Formal analysis; Investigatio; Supervision; Visualization; Roles/Writing - original draft; Writing - review & editing. ***Waleed I. M. El-Azab**:* Conceptualization; Supervision; Visualization; Roles/Writing - original draft; Writing - review & editing. ***Mohamed A. Ebiad**:* Conceptualization; Supervision; Visualization; Writing - review & editing

Authors' information:

Authors and Affiliations

a- Analysis & Evaluation Division, Egyptian petroleum research institute, Nasr city, Cairo 11727, Egypt

Ayat A.-E. Sakr, Mohamed Bakry, Waleed I. M. El-Azab, and Mohamed A. Ebiad.

b- **Faculty of Biotechnology, October University for Modern Sciences and Arts (MSA), Egypt.**

Nouran Amr

Corresponding author:

(Ayat. A.-E. Sakr); Email: ayatsakr@yahoo.com; ayatsakr78@gmail.com; ayatsakr@epri.sci.eg.

Data availability: All related data and materials are within the manuscript.

Declarations

Ethics approval and consent to participate: The authors have approved and participated in the manuscript.

Consent for publication: Publication has been approved by the authors.

Conflict of interest: The authors declare no competing interests.

References

Alhawi T, Rehan M, York D, Lai X (2015) Hydrothermal Synthesis of Zinc Carbonate Hydroxide Nanoparticles. Procedia Eng 102:356–361. https://doi.org/10.1016/j.proeng.2015.01.161

Baghbanzadeh M, Carbone L, Cozzoli PD, Kappe CO (2011) Microwave-Assisted Synthesis of Colloidal Inorganic Nanocrystals. Angew Chem Int Ed 50:11312–11359. https://doi.org/10.1002/anie.201101274

Bitenc M, Marinšek M, Crnjak Orel Z (2008) Preparation and characterization of zinc hydroxide carbonate and porous zinc oxide particles. J Eur Ceram Soc 28:2915–2921. https://doi.org/10.1016/j.jeurceramsoc.2008.05.003

Bocos-Bintintan V, Ratiu IA (2020) Hunting for Toxic Industrial Chemicals : Real-Time Detection of Carbon Disulfide Traces by Means of Ion Mobility Spectrometry Victor. Toxics 8:121

Boyd GE, Adamson a W, Myers LS (1947) The exchange adsorption of ions from aqueous solutions by organic zeolites; kinetics. J Am Chem Soc 69:2836–2848.

https://doi.org/10.1021/ja01203a066

BP (2022) BP Energy Outlook: 2022 edition. BP p.l.c

Bundit O, Wongsaprom K (2018) Shape control in zinc oxide nanostructures by precipitation method. J Phys Conf Ser 1144:012044

Cao Z, Wei G, Zhang H, et al (2020) Adsorption Property of CS2 and COF2 on Nitrogen-Doped Anatase TiO2(101) Surfaces: A DFT Study. ACS Omega 5:21662–21668. https://doi.org/10.1021/acsomega.0c02499

Chen DZ, Zhang JX, Chen JM (2010) Adsorption of methyl tert-butyl ether using granular activated carbon: Equilibrium and kinetic analysis. Int J Environ Sci Technol 7:235–242. https://doi.org/10.1007/BF03326133

Chen X, Shen B, Sun H, et al (2017) Adsorption and Its Mechanism of CS2 on Ion-Exchanged Zeolites Y. Ind Eng Chem Res 56:6499−6507. https://doi.org/10.1021/acs.iecr.7b00245

D5623 (2004) Standard Test Method for Sulfur Compounds in Light Petroleum Liquids by Gas. In: ASTM standards. ASTM International, pp 1–6

Dan H, Honghong Y, Xiaolong T, et al (2012) The catalytic hydrolysis of carbon disulfide on Fe–Cu–Ni/AC catalyst at low temperature. J Mol Catal A Chem 357:44–49. https://doi.org/10.1016/j.molcata.2012.01.017

DeMartino AW, Zigler DF, Fukuto JM, Ford PC (2017) Carbon disulfide. Just toxic or also bioregulatory and/or therapeutic? Chem Soc Rev 46:21–39. https://doi.org/10.1039/c6cs00585c

Doğan M, Karaoğlu MH, Alkan M (2009) Adsorption kinetics of maxilon yellow 4GL and maxilon red GRL dyes on kaolinite. J Hazard Mater 165:1142–1151. https://doi.org/10.1016/j.jhazmat.2008.10.101

Ebelegi AN, Ayawei N, Wankasi D (2020) Interpretation of Adsorption Thermodynamics and Kinetics. Open J Phys Chem 10:166–182. https://doi.org/10.4236/ojpc.2020.103010

Ebiad MA, El-hafiz DRA, Masod MB (2020) β -FeOOH/C nanocomposite for elemental mercury removal as a new approach to environmental and natural gas processes. J Nat Gas Sci Eng 80:103383. https://doi.org/https://doi.org/10.1016/j.jngse.2020.103383

EIA (2021) International Energy Outlook 2021 Narrative. U.S. Energy Information Administration

El-Sharabasy SF, Rizk RM (2019) Atlas of date palm in Egypt. Food and Agriculture Organization of the United Nations (FAO), Egypt

Faramawy S, Zaki T, Sakr AAE, et al (2018) The activity of Mg-Al layered double hydroxides intercalated with nitrogen-containing anions towards the removal of carbon dioxide from natural gas. J Nat Gas Sci Eng 54:72–82. https://doi.org/10.1016/j.jngse.2018.04.002

Fernández Y, Menéndez JA, Arenillas A, et al (2009) Microwave-assisted synthesis of CuO / ZnO and CuO / ZnO / Al 2 O 3 precursors using urea hydrolysis. Solid State Ionics 180:1372–1378. https://doi.org/10.1016/j.ssi.2009.08.014

Frilund C, Simell P, Kaisalo N, et al (2020) Desulfurization of Biomass Syngas Using ZnO-Based Adsorbents: Long-Term Hydrogen Sulfide Breakthrough Experiments. Energy Fuels 3316−3325. https://doi.org/10.1021/acs.energyfuels.9b04276

Georgiadis AG, Charisiou ND, Goula MA (2020) Removal of Hydrogen Sulfide From Various Industrial Gases: A Review of The Most Promising Adsorbing Materials. Catalysts 10:521

Ghenaatian HR, Baei MT, Hashemian S (2013) Zn12O12 nano-cage as a promising adsorbent for CS2 capture. SUPERLATTICES Microstruct 58:198–204. https://doi.org/10.1016/j.spmi.2013.03.006

Giannakoudakis DA, Arcibar-orozco JA, Bandosz TJ (2015) Key role of terminal hydroxyl groups and visible light in the reactive adsorption/catalytic conversion of mustard gas surrogate on zinc (hydr) oxides. Appl Catal B Environ 175:96–104

Giannakoudakis DA, Bandosz TJ (2014) Zinc (hydr) oxide/graphite oxide/AuNPs composites: Role of surface features in H2S reactive adsorption. J Colloid Interface Sci 436:296–305. https://doi.org/10.1016/j.jcis.2014.08.046

Gordeeva A, Hsu Y, Jenei IZ, et al (2020) Layered zinc hydroxide dihydrate , Zn5(OH)10·2H2O, from hydrothermal conversion of ε-Zn (OH)2 at gigapascal pressures and its transformation to nanocrystalline ZnO. ACS Omega 5:17617−17627. https://doi.org/10.1021/acsomega.0c02075

Guo B, Chang L, Xie K (2006) Study of the behavior of adsorbing CS2 by activated carbon. Fuel Process Technol 87:873–881. https://doi.org/10.1016/j.fuproc.2006.06.001

Guo Y, Chang B, Wen T, et al (2016) One-pot synthesis of graphene/zinc oxide by microwave irradiation with enhanced supercapacitor performance. RSC Adv 6:19394–19403. https://doi.org/10.1039/c5ra24212f

Haggag EA, Masod MB, Abdelsamad AA, et al (2021) Kinetic studies on the adsorption of uranium on a mesoporous impregnated activated carbon. Egypt J Chem 64:1371–1385. https://doi.org/10.21608/EJCHEM.2020.50611.3039

Han Y, Quan X, Chen S, et al (2006) Electrochemically enhanced adsorption of phenol on activated carbon fibers in basic aqueous solution. J Colloid Interface Sci 299:766–771. https://doi.org/10.1016/j.jcis.2006.03.007

Han Y, Zhang Y, Xu C, Hsu CS (2018) Molecular characterization of sulfur-containing compounds in petroleum. Fuel 221:144–158

Ho YS, Mckay G (1999) Pseudo-second order model for sorption processes. Process Biochem 34:451–465

Hsu CS, Robinson PR (eds) (2017) Springer Handbook Petroleum Technology. Springer International Publishing AG

Iruretagoyena D, Montesano R (2018) Selective Sulfur Removal from Liquid Fuels Using Nanostructured Adsorbents. In: Saleh TA (ed) Nanotechnology in Oil and Gas Industries: Principles and Applications. Springer International Publishing AG

Kloprogge JT, Hickey L, Frost RL (2004) FT-Raman and FT-IR spectroscopic study of synthetic Mg / Zn / Al-hydrotalcites. 967–974

Kloprogge JT, Hickey L, Trujillano R, et al (2006) Characterization of intercalated Ni/Al hydrotalcites prepared by the partial decomposition of urea. Cryst Growth Des. https://doi.org/10.1021/cg0504612

Kohl AL, Nielsen RB (eds) (1997) Gas Purification, 5th edn. Gulf Publishing Company, Houston, Texas

Kowalik P, Bicki R, Antoniak-Jurak K, et al (2020) Preparation and evaluation of active Cu-Zn-Al mixed oxides to CS2 removal for CO2 ultra-purification. J Hazard Mater 398:122737.

https://doi.org/10.1016/j.jhazmat.2020.122737

Lagergren S (1898) About the theory of so-called adsorption of soluble substances. 1–39

Li K, Li K, Wang C, et al (2020) Preparation of polyacrylonitrile-based activated carbon fiber for CS2 adsorption. Res Chem Intermed 46:3459–3476. https://doi.org/10.1007/s11164-020-04156-1

Liu N, Ning P, Sun X, et al (2021) Simultaneous catalytic hydrolysis of HCN , COS and CS2 over metal-modified microwave coal-based activated carbon. Sep Purif Technol 259:118205. https://doi.org/10.1016/j.seppur.2020.118205

Ma X, Velu S, Kim JH, Song C (2005) Deep desulfurization of gasoline by selective adsorption over solid adsorbents and impact of analytical methods on ppm-level sulfur quantification for fuel cell applications. Appl Catal B Environ 56:137–147. https://doi.org/10.1016/j.apcatb.2004.08.013

Mantovani KM, Stival JF, Wypych F, et al (2017) Unusual catalytic activity after simultaneous immobilization of two metalloporphyrins on hydrozincite/nanocrystalline anatase. J Catal 352:442–451. https://doi.org/10.1016/j.jcat.2017.06.015

Mavis B, Akinc M (2006) Kinetics of Urea Decomposition in the Presence of Transition Metal Ions: Ni2+. J Am Ceram Soc 89:471–477. https://doi.org/10.1111/j.1551-2916.2005.00758.x

McGuirk CM, Siegelman RL, Drisdell WS, et al (2018) Cooperative adsorption of carbon disulfide in diamine-appended metal–organic frameworks. Nat Commun 9:5133. https://doi.org/10.1038/s41467-018-07458-6

Molefe F V, Koao LF, Dejene BF, Swart HC (2015) Phase formation of hexagonal wurtzite ZnO through decomposition of Zn(OH)2 at various growth temperatures using CBD method. Opt Mater (Amst) 46:292–298

Montero-Campillo MM, Alkorta I, Elguero J (2018) Binding indirect greenhouse gases OCS and CS2 by nitrogen heterocyclic carbenes (NHCs). Phys Chem Chem Phys 20:19552–19559. https://doi.org/10.1039/c8cp03217c

Orhan OY, Cihan FN, Alper E (2019) Kinetics and mechanism of reaction between carbon disulfide and novel aqueous amines solutions. Int J Glob Warm 18:401–409. https://doi.org/10.1504/IJGW.2019.101078

608 Padmanabhan SC, Ledwith D, Pillai SC, et al (2009) Microwave-assisted synthesis of ZnO micro-
609 javelins. J Mater Chem 19:9250–9259. https://doi.org/10.1039/B912537J

610 Qiu T, Yang J, Bai X, Wang Y (2019) The preparation of synthetic graphite materials with hierarchical
611 pores from lignite by one-step impregnation and their characterization as dye absorbents. RSC
612 Adv 9:12737–12746. https://doi.org/10.1039/c9ra00343f

613 Ramimoghadam D, Bin-Hussein MZ, Taufiq-Yap YH (2013) Hydrothermal synthesis of zinc oxide
614 nanoparticles using rice as soft biotemplate. Chem Cent J 136:1–10

615 Reichenberg D (1953) Ion-Exchange Resins in Relation to their Structure. III. Kinetics of Exchange. J
616 Am Chem Soc 75:589–597

617 Rhodes C, Riddel SA, West J, et al (2000) The low-temperature hydrolysis of carbonyl sulfide and
618 carbon disulfide: a review. Catal Today 59:443–464

619 Rich AL, Patel JT, Al-Angari SS (2016) Carbon Disulfide (CS2) Interference in Glucose Metabolism
620 from Unconventional Oil and Gas Extraction and Processing Emissions. Environ Health Insights
621 10:51–57. https://doi.org/10.4137/EHI.S31906

622 Saber O, Tagaya H (2005) PREPARATION OF NEW LAYERED DOUBLE HYDROXIDE ,. 10:

623 Sadare OO, Obazu F, Daramola MO (2017) Biodesulfurization of Petroleum Distillates — Current
624 Status, Opportunities and Future Challenges. Environments 4:85.
625 https://doi.org/10.3390/environments4040085

626 Sahibed-Dine A, Aboulayt A, Bensitel M, et al (2000) IR study of CS2 adsorption on metal oxides:
627 relation with their surface oxygen basicity and mobility. J Mol Catal A Chem 162:125–134

628 Sakr AA-E, Zaki T, Elgabry O, et al (2021) Enhanced CO2 capture from methane-stream using MII -
629 Al LDH prepared by microwave-assisted urea hydrolysis. Adv Powder Technol 32:4096–4109.
630 https://doi.org/10.1016/j.apt.2021.09.016

631 Sakr AA-E, Zaki T, Saber O, et al (2013) Synthesis of Zn–Al LDHs intercalated with urea derived
632 anions for capturing carbon dioxide from natural gas. J Taiwan Inst Chem Eng 44:957–962.
633 https://doi.org/10.1016/j.jtice.2013.02.003

634 Sakr AAE, Zaki T, Elgabry O, et al (2018) Mg-Zn-Al LDH: Influence of intercalated anions on CO2

removal from natural gas. Appl Clay Sci 160:263–269. https://doi.org/10.1016/j.clay.2018.02.043

Saleh A (2020) Characterization, determination and elimination technologies for sulfur from petroleum: Toward cleaner fuel and a safe environment. Trends Environ Anal Chem 25:e00080

Seredych M, Mabayoje O, Koleśnik MM, et al (2012) Zinc(hydr)oxide/graphite based-phase composites: effect of the carbonaceous phase on surface properties and enhancement in electrical conductivity. J Mater Chem 7970–7978. https://doi.org/10.1039/c2jm15350e

Shaw BWHR, Bordeaux JJ (1955) The Decomposition of Urea in Aqueous Media. J Am Chem Soc 77:4729

Speight JG (ed) (2011) The Refinery of the Future, 1st edn. Gulf Professional Publishing-Elsevier Inc.

Stumpf Á, KrisztinaTolvaj, Juhász M (1998) Detailed analysis of sulfur compounds in gasoline range petroleum products with high-resolution gas chromatography – atomic emission detection using group-selective chemical treatment. J Chromatogr A 819:67–74

Swat AAA, Saleh TA, Ganiyu SA, et al (2017) Preparation of activated carbon , zinc oxide and nickel oxide composites for potential application in the desulfurization of model diesel fuels. J Anal Appl Pyrolysis 128:246–256. https://doi.org/10.1016/j.jaap.2017.10.004

UN (2015) Transforming our world: the 2030 agenda for sustainable development. A/RES/70/1. United Nations

Verges MA, Mifsud A, Serna CJ (1990) Formation of rod-like zinc oxide microcrystals in homogeneous solutions. J Chem Soc Faraday Trans 86:959–963

Wang F, Chen H, Sun X, et al (2021) Single atom Fe in favor of carbon disulfide (CS2) adsorption and thus the removal efficiency. Sep Purif Technol 258:118086. https://doi.org/10.1016/j.seppur.2020.118086

Wang F, Wang X, Ning P, et al (2015) Adsorption of carbon disulfide on activated carbon modified by Cu and cobalt sulfonated phthalocyanine. Adsorption 21:401–408. https://doi.org/10.1007/s10450-015-9680-x

Wang H, Wang FY, Wang H, Ma JW (2010) Adsorption of Cadmium (II) Ions from Aqueous Solution

662 by a New Low-Cost Adsorbent – Bamboo Charcoal. J Hazard Mater 177:300–306.
663 https://doi.org/10.1016/j.jhazmat.2009.12.032

664 Wang L, Guo Y, Lu G (2011) Effect of activated carbon support on CS 2 removal over coupling
665 catalysts. 20:397–402. https://doi.org/10.1016/S1003-9953(10)60197-1

666 Wang XQ, Wang F, Chen W, et al (2014) Adsorption of Carbon Disulfide on Cu/CoSPc/Ce Modified
667 Activated Carbon under Microtherm and Micro-oxygen Conditions. Ind Eng Chem Res
668 53:13626−13634. https://doi.org/10.1021/ie5016443

669 Weber WJ, Morris JC (1963) Kinetics of adsorption on carbon from solution. J Sanit Eng Div 89:31–
670 60

671 WHO (2002) Concise International Chemical Assessment Document 46: CARBON DISULFIDE.
672 Geneva, Switzerland

673 Xie Z, Wang F, Zhao N, et al (2011) Hydrophobisation of activated carbon fiber and the influence on
674 the adsorption selectivity towards carbon disulfide. Appl Surf Sci 257:3596–3602.
675 https://doi.org/10.1016/j.apsusc.2010.11.085

676 Yang J, Juan P, Shen Z, et al (2006) Removal of carbon disulfide (CS 2) from water via adsorption on
677 active carbon fiber (ACF). 44:1367–1375. https://doi.org/10.1016/j.carbon.2005.11.016

678 Yi H, Zhao S, Tang X, et al (2014) Deactivation and reactivation of the KOH impregnated Fe–Cu–
679 Ni/AC catalyst for hydrolysis of carbon disulfide. Catal Commun 56:106–109.
680 https://doi.org/10.1016/j.catcom.2014.06.031

681 Youssef AM, Ahmed AI, Amin MI, El-Banna U a. (2014) Adsorption of lead by activated carbon
682 developed from rice husk. Desalin Water Treat 3994:1–14.
683 https://doi.org/10.1080/19443994.2014.896289

684 Youssef AM, Hassan AF, Ebiad MA, Bakry M (2016) Adsorption of Hg 2+ using modified sulfur-
685 impregnated activated carbon from olive stone. Mansoura J Chem 42:16

686 Zhang H, Feng J, Wang J, Zhang M (2007) Preparation of ZnO nanorods through wet chemical
687 method. Mater Lett 61:5202–5205. https://doi.org/10.1016/j.matlet.2007.04.030

688 Zhang SC, Li XG (2003) Preparation of ZnO particles by precipitation transformation method and its

689 inherent formation mechanisms. Colloids Surfaces A Physicochem Eng Asp 226:35–44.
690 https://doi.org/10.1016/S0927-7757(03)00383-2
691

Supplementary Files

This is a list of supplementary files associated with this preprint. Click to download.

- suppinfA.docx